Journal of Materials Chemistry C

ROYAL SOCIETY OF CHEMISTRY

PAPER

View Article Online
View Journal

Cite this: DOI: 10.1039/d6tc00969g

Deconvoluting the electronic landscape of ZnO using 2D excitation–emission spectroscopy: effects of microstructuring, doping and restructuring

Daniel J. Oliver,† Victor V. Volkov† and Carole C. Perry *

Understanding the electronic properties and energy relaxation pathways of semiconductors, is essential for developing next-generation materials for applications in areas as diverse as medicine, flat panel-displays and sensing. In this contribution we apply two-dimensional excitation–emission spectroscopy to interpret energy relaxation pathways in pure and biohybrid zinc oxide (ZnO) micro- and nanostructures of differing morphologies and evaluate the effects of chemical processing and plasmonic doping. In pure ZnO microcrystals with low surface-to-volume ratio, ultraviolet near-band-edge exciton emission dominates relaxation. In contrast, ZnO nanorods, with high surface-to-volume ratio exhibit strong red and near-infrared emission we ascribe to zinc interstitials, oxygen vacancies, and oxygen interstitial defects. Hybrid ZnO structures display a redistribution of energy flow to yield a distinctly different set of red and green emissions stimulated from lower energy states we assign to extended zinc interstitials, oxygen vacancies, and zinc vacancies. Post-synthetic modification preferentially attenuates lower-energy donor states, thereby enhancing higher-energy emission channels. For treatment with polyvinyl alcohol we discuss the role of hydroxyl groups in the restructuring of surface interstitial defects and passivation of negative zinc vacancies, while borohydride treatment can stimulate reduction-driven compensation of positively charged defects and hydrogen ion diffusion. Application of two-dimensional spectral analysis is critically important to avoid ambiguity in evaluation of electronic properties of semiconductors such as zinc oxide and materials with complex networks of energy relaxation pathways.

Received 25th March 2026,
Accepted 14th May 2026

DOI: 10.1039/d6tc00969g

rsc.li/materials-c

1. Introduction

Zinc oxide (ZnO) is a II–VI semiconductor with a band gap of *ca.* 3.3 eV, whose properties have been widely studied for at least the past 7 decades.[1–5] The wurtzite polymorph is known for its structural diversity with respect to native defect states. Depending upon the preparation technique, single crystals,[6] thin films,[7] wires,[8] nanocrystals[9] and nanobelts[10] can be formed each with different electronic and optical properties. The tunable optical and luminescence characteristics of ZnO[11–13] make the II–VI semiconductor suitable for a range of applications which include: medicine,[14,15] engineering novel electronics,[16–18] flat-panel displays[13] and sensing devices.[19,20]

ZnO emissions can be divided into two regions: ultraviolet (UV) and visible emissions. Typically, UV spectra of ZnO bulk and film samples demonstrate discrete narrow sets of spectral signatures specific to band-gap excitons (of variant nature) and closely associated transitions.[21,22] In the visible spectral range, ZnO materials can emit relatively broad spectral components, which are often categorized as 'green',[13,23,24] 'blue',[25] 'yellow',[25,26] and 'red'.[27] Visible emissions are attributed to native deep and/or shallow trap defects that stimulate conduction band (CB) → trap and trap → valence band (VB) luminescent transitions of different colors according to the energy levels of the involved trapping defects.[23] The ability to tune the spectral emission of ZnO with no additional dopants solely through controlling defect/trap state populations is attractive for a range of optoelectronic applications including solar cells,[28] and light emitting diodes.[29] While most of the tunable emission resides within the visible range, low energy transitions have been reported to produce emission in the near infrared region.[30]

Within the past 2 decades, significant progress has been made in the preparation of ZnO nanomaterials with nanoplasmonic inclusions:[31–36] ZnO-Au hybrid structures may provide high efficiency photovoltaic[37] and photocatalytic[38–41] devices, as well as acting as sensors to demonstrate effective

Interdisciplinary Biomedical Research Centre, School of Science and Technology, Nottingham Trent University, Clifton Lane, Nottingham NG11 8NS, UK.
E-mail: carole.perry@ntu.ac.uk
† Both authors contributed equally.

Surface Enhanced Raman Scattering.[42–45] Typically, zinc oxide (ZnO) nano and micro assemblies and gold (Au) nanoparticles are the constituents. In our recent studies,[46] we presented a novel one-pot approach to prepare ZnO–ZA2–Au materials, where the Au nano-inclusions are embedded within the ZnO material due to using a hybrid polypeptide sequence GLHVMH KVAYSSGAPPMPPF (ZA2) to link the two phases. Modeling optical absorption properties of ZnO–ZA2–Au composites suggested hybrid materials may contribute to microelectronics engineering and affect Ohmic contact processes.[47]

Both prediction and effective control of the electronic properties of ZnO materials by means of synthesis procedure, doping or material combinatorics requires adequate characterization of the resulting electronic properties. In a recent paper,[48] we showed that when we address semiconductors with intricate energy relaxation pathways, application of conventional emission spectroscopy may be insufficient for both the qualitative assignment of transitions and quantitative evaluation of quantum yield. We approached the problem using fitting of two-dimensional excitation–emission matrices (2DEM) of emission spectra assembled according to excitation wavelengths. We showed that the approach has promise to be able to resolve energy relaxation networks in systems like ZnO, where emission components present a complex superimposition due to transitions of different nature.

In this contribution we demonstrate how two-dimensional excitation–emission spectral analysis may help to sort and quantify competing relaxation pathways present in ZnO materials according to synthesis conditions that affect oxide crystallinity, surface to volume ratio, and morphology of macro-assemblies. Specifically, our library of ZnO materials includes an analytical standard, microspheres,[49] nanorods, polypeptide mediated nanoplatelets and nanoflowers,[50,51] as well as ZnO–ZA2–Au composites.[47] The nanoplatelet, nanoflower and ZnO–ZA2–Au composite samples were selected to explore possible effects of material combinatorics to involve polypeptide mediated material structuring and plasmonic inclusions. To address effects of post synthetic modifications of electronic states, we also treat the samples with 0.5% polyvinyl alcohol (PVA),[52] to effect surface passivation and with 1 M $NaBH_4$ which is reported to increase oxygen vacancies at the surface.[53]

The outline of the paper is as follows: first, we review the structural and material properties of the chosen samples; second, we present a general outline for the results of two-dimensional excitation emission spectroscopy; next, according to spectral analysis and literature precedence we address the ladder of energy states specific to ZnO materials and specify the diversity of energy relaxation pathways quantitatively. Subsequently, we discuss contributions of specific defects in the energy relaxation of ZnO in dependence on structure, possible confinement, and chemistry imposed by external reactants. Application of two-dimensional spectral analysis is critically important to avoid ambiguity in evaluation of electronic properties of semiconductors such as zinc oxide and materials with complex networks of energy relaxation pathways.

2. Materials and methods

Details of the materials purchased, the preparation of ZnO samples and their post-synthesis treatment with sodium borohydride or polyvinyl alcohol (PVA) are described in the SI.

2.1. Materials characterization: size, morphology, and structure

Structural properties of the ZnO samples were determined using SEM microscopy JEOL JSM-7100F (JEOL Ltd., Akishima, Japan) at an accelerating voltage of 5 keV. SEM SEI imaging was used to determine the size and morphology of uncoated samples with at least 50 particles being measured for each sample. For the ZnO–ZA2–Au sample a JEOL 2100 Plus TEM/STEM microscope fitted with a JEOL EX-24200M1G2T EDX system (JEOL Ltd., Akishima, Japan) and a LaB_6 source was used to study the nanoscale gold inclusions as described in ref. 47.

Further structural and composition-based information was determined using a PANalytical X'Pert PRO X-ray diffractometer (Malvern Panalytical Ltd. Malvern, UK) having Cu Kα radiation operating at a wavelength of 1.54056 Å. The samples were scanned over a range between 3° and 90° of 2θ with a step size of $0.02^\circ\ s^{-1}$. Experiments were carried out at room temperature with an acceleration voltage of 45 kV and 40 mA filament current. The X'Pert-HighScore Plus 4.5 (Malvern Panalytical Ltd. Malvern, UK) program was used to analyse and identify peaks in the diffraction patterns, for the line spectra see Fig. S1 in SI. The crystallite domain size was determined according to the Scherrer formula[54] with the following constants: X-ray wavelength 0.15406 nm & shape factor (K) of 0.9, while B was determined at the full width half maximum.

2.2. Two-dimensional excitation emission spectroscopy and analysis

All fluorescence measurements of bulk samples were performed using a TECAN i-control M200 Pro spectrometer (Tecan Group Ltd. Switzerland) fitted with a monochromator and controlled by the i-control (version 1.9.17.0) software, and black 96-well plates (Corning Inc., Corning, New York USA) to hold solid-state samples. Spectral analysis was conducted following a fitting procedure, as described previously.[48] Initial parameters for adopted transitions and line-shapes are according to literature values[11,12,55] and to ensure consistency across all the samples considered. When discussing emissive contributions of electronic states for different ZnO materials, it is useful to express quantum yields for transitions to allow for easier comparison of this data with future studies which may use different spectrometers or have a different experimental setup. To express relative quantum yields of a sample we normalize the contribution of each emissive component by the sum of the contributions of all emissions as detected for the sample. These relative quantum yields are helpful to describe how different pathways of a sample contribute to energy relaxation. Comparing the relative quantum yields of quantified pathways for

different samples, we may discuss the role of structure and material compositions on energy relaxation.

2.3. Evaluation of absolute quantum yields

Relative quantum yields do not describe if a pathway of interest for a certain material would be a better emitter than a pathway of another material. To evaluate absolute values, we compare emission efficiencies against rhodamine 6G[56] while weighting proportions for significantly diluted powder samples (in spectroscopic grade KBr) to confirm optical absorbance values for ZnO and R6G dye which are approximately equal at 515 nm. The evaluations are approximate since we assume the same amount of matter with the same surface to volume ratio and the same density of emitting states.

3. Results

3.1. Material properties

Fig. 1 presents images and size distributions for the pure ZnO (upper row of panels) and hybrid (lower row of panels) structures included in this study. The SI file Fig. S1 and S2 present X-ray data and low frequency Raman spectra for selected samples. The data indicates dominance of relatively well-established lattices in the prepared systems, save in the case of microspheres, where vibrational spectroscopy suggests structural irregularities.[57,58]

Among the pure Zinc oxide polycrystalline materials, the analytical standard sample comprises nonsymmetrical semi-spherical particles with average size of 117 μm: see representative SEM image and size histogram in Fig. 1(1). In contrast, ZnO microspheres are of relatively regular, symmetric shape with average diameter about 1.9 ± 0.4 μm, Fig. 1(2) and exhibit a large reduction in crystalline domain size (see Table 1) and deviation of vibrational properties: see Fig. S2 in the SI file. The third, ZnO sample, twinned ZnO nanorods have an average length of 1.4 ± 0.2 μm with a length to diameter ratio (*L*/*D*) of 10.7 ± 1.7: see Fig. 1(3). For the ZnO standard, microsphere and nanorod samples, Table 1 suggests a ratio of the outer surface to internal interdomain surface to increase from about 0.001 to 0.02 and to 0.6, respectively. We compute these values approximating a domain and a particle volume (to fill) to be under rectangular cuboid geometry.

Table 1 ZnO & Au domain sizes calculated using the Scherrer equation[54] with corresponding particle size for each sample as well as ratio of the outer surface to the inter domain surface

Sample components	Particle/ assembly size (μm)	Domain size (nm)	Outer surface to inter-domain surface
Standard: ZnO	117 ± 38	52 ± 9	0.001 ± 0.0005
Microsphere: ZnO	1.9 ± 0.4	18 ± 5	0.02 ± 0.01
Nanorod: ZnO	1.4 ± 0.2	23 ± 7	0.6 ± 0.06
Platelet (GT16): ZnO	0.8 ± 0.1	18 ± 2	0.14 ± 0.04
Flower (ZA2): ZnO	5.4 ± 0.3	46 ± 6	0.68 ± 0.36
ZnO–ZA2–Au: ZnO	5.0 ± 0.3	45 ± 4	0.23 ± 0.11
ZnO–ZA2–Au: Au	0.019 ± 0.007	19 ± 6	

In the group of hybrid ZnO based systems, related by synthesis protocol,[50,51,55] the nanoplatelets have an average diameter of 0.8 ± 0.1 μm and a *L*/*D* of 0.2 ± 0.1 μm, and the flower like assemblies have an average diameter of 5.4 ± 0.3 μm: see Fig. 1(4) and (5), respectively. The flowers consist of nanorod-like structures, which stem from a common centre. The length of each such nanorod is about 1.7 ± 0.1 μm with *L*/*D* ratio of 3.7 ± 0.4. For the platelets and nanorods of the flower assemblies, the domain size data, Table 1 suggests the ratio of the outer surface to internal inter-domain surface to increase from about 0.14, to 0.68, respectively.

The last sample, ZnO microparticles with Au inclusions. SEM image and histogram of sizes in Fig. 1(6) suggest pseudo-spherical micro-assemblies with average diameter of 5.0 ± 0.3 μm, while TEM images the SI file describe the assemblies to contain discrete nanoscale gold inclusions to be distributed quite uniformly in the ZnO hosting matrix.[46] Data in Table 1 list the domain size for gold nano-inclusions in ZnO–ZA2–Au systems to be 19 ± 7 nm, comparable with the average gold nanoparticle diameter. This suggests the metal component to demonstrate well an established lattice that corresponds with diffractograms for ZnO–ZA2–Au accounting $Au_{(111)}$, $Au_{(200)}$ & $Au_{(220)}$ peaks: see Fig. S1 in the SI file. For this sample, with the merged rod-like structural elements to demonstrate length and width to vary 1200 ± 200 and 250 ± 50 nm, respectively, the ratio of the outer surface to internal inter-domain surface is about 0.23. This is comparable with the ratios we anticipate for the other biohybrid composites.

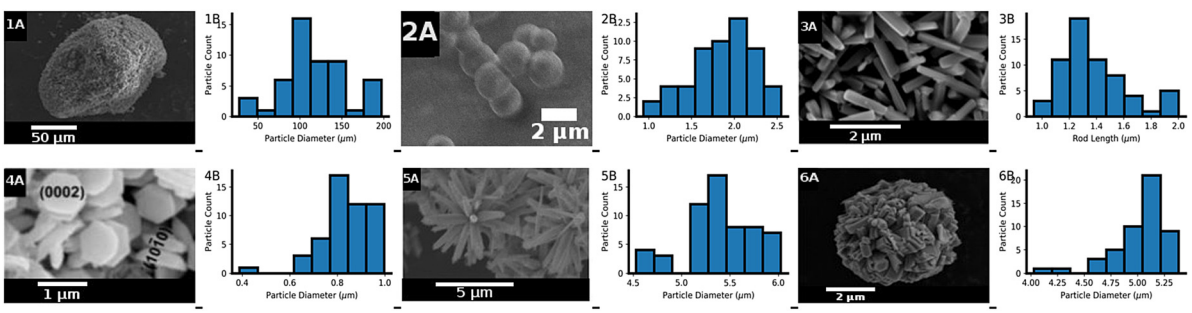

Fig. 1 Representative scanning electron microscopy (SEM) micrographs (A) and size distribution data determined from multiple areas (B) for the ZnO library: The numbers denote: (1) analytical standard, (2) microspheres, (3) nanorods, (4) nanoplatelets, (5) nanoflowers & (6) ZnO–ZA2–Au composite.

3.2. ZnO two-dimensional excitation emission spectra

The upper set of panels in Fig. 2 present data for the considered materials as prepared and treated with PVA or $NaBH_4$. The spectra suggest a wide diversity of energy relaxation pathways in the selected materials. With excitation varying from 300 to 600 nm, the experimental data exhibit intricate convolutions of emission bands detected in the wavelength range from 350 to 800 nm.

To take advantage of the 2D format, which orders emission spectra in respect to excitation wavelength, we conduct numerical fitting of the experimental spectra (see Fig. S4–S6 in SI file) according to procedures and software as described previously.[48] Comparing the results of fitting we generalize the energy ladder manifold specific to ZnO based materials (see the lower set in Fig. 2). The developed manifold offers a template to facilitate/speed-up a quantitative review of the diversity of energy relaxation pathways in such materials. Of course, this is according to the spectral resolution as present in experiment: for example, optical phonon progressions under line narrowing at liquid helium temperature are not in the scope of our resolution at room temperature.

Factoring of the detected emission is not trivial because both radiative and non-radiative channels may compete and combine. A search for the proper ladder of emitting states can be facilitated by the following instructions: (i) the electronic-state characteristics of different samples are relevant[59–70] in respect to complementary theoretical work,[71–76] (ii) diagonal emissive components (with close excitation and emission wavelengths) are direct measures of the ladder states, particularly helpful for identification of in-gap donor trap states,

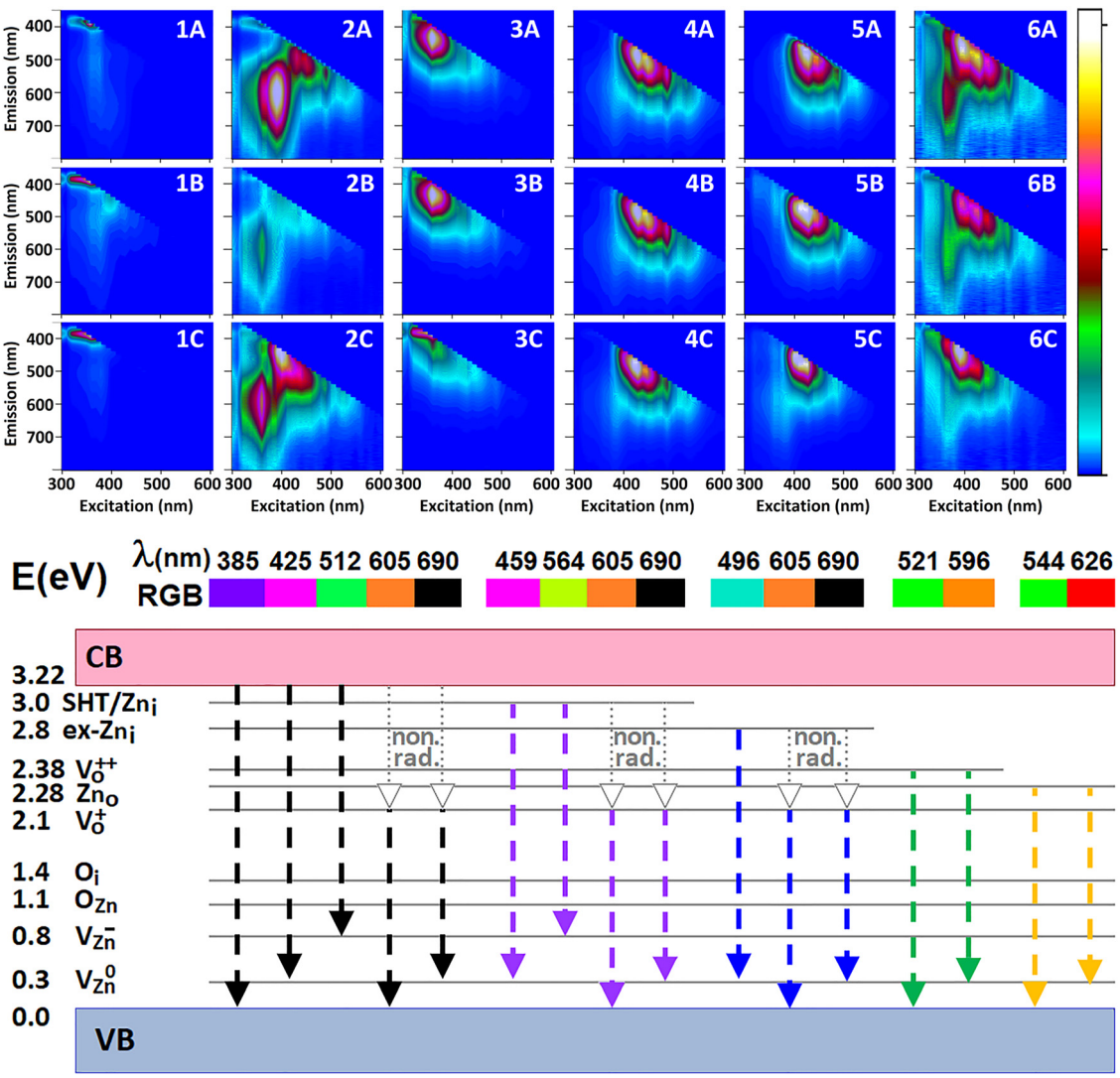

Fig. 2 Upper set: 2D spectra of the ZnO library (A), 0.5% PVA treated (B) and 1 M $NaBH_4$ treated (C). The numbers denote: (1) analytical standard, (2) nanorods, (3) microspheres, (4) nanoplatelets, (5) nanoflowers & (6) ZnO–ZA2–Au composite. Lower set: energy relaxation diagram we generalise according to our 2D spectroscopy fitting to account emissive components specific to Band Gap/Exciton, ultraviolet, blue, green and yellow excited groups of emission and non-radiative (non. rad.) relaxation, as observed in the considered ZnO based microstructures: Discussion in the main text provides further specifications.

(iii) fitting the 2D line-shapes is constrained by the dephasing limit width (since the lack of coherence) along the excitation axis, (iv) sample modifications only redistribute energy to flow according to the same ZnO specific ladder manifold, (v) all detected transitions under different excitation wavelengths must agree with energy differences between donor and acceptor states of the same ladder manifold.

In the SI file, we present a detailed assignment outline of the energy ladder we developed accounting: (1) fitting of 2D convolved spectral components as observed under different excitations, (2) discussions of experimental outcome as reported in literature and (3) suggestions of theoretical studies. Fig. S9 in the SI presents examples to show that fitting conventional 1D spectra (which are slices from naturally present convolutions) cannot help in the identification of the transitions involved due to convolution of neighbouring (along the excitation axis) relaxation contributions.

According to our review of the energy ladder to confirm the detected 2D spectral signatures, we conclude that the two-dimensional spectra do not support discussion on a unique source of a "green", or "blue", "red" emission. Instead, the approach offers quantitative sorting to specify how the energy manifold (specific to ZnO based materials in this case) may sustain pathways under different excitations to yield emissions of similar colors. Accordingly, we demonstrate that ZnO may emit similar color "green" or "blue" emissions due to different relaxation pathways under different excitations. Two-dimensional spectroscopy allows such contributions to be included with Fig. 2B showing a pictorial example of the approach for the systems studied. Furthermore, fitting 2D spectra we may review and compare energy relaxation diagrams for different ZnO systems and on the effect of external perturbations, as we present in Fig. 3–5. The observed alterations in energy relaxation pathways are related to the structure of the materials themselves and to their mode of formation and further treatment as we discuss below.

For example, considering Fig. 2(1A), we may clearly see that UV emission at *ca.* 372 nm (3.33 eV) is dominant for the analytical standard, while ZnO nanorods (Fig. 2(2A)) demonstrate a rich palette of emitting components with main emission in the visible spectral range to account so-known 'red' and 'green' luminescence at about 605 and 496 nm, which are typically attributed to surface associated traps in ZnO.[77] In the case of microspheres (Fig. 2(3A)), the unusually blue shifted signature at about 425 nm governs the spectrum. The spectra of the ZnO-polypeptide hybrid materials (Fig. 2(4A) and (5A)) exhibit relatively compact line shapes (in terms of 2D bandwidth), but shifted from 500 to 600 nm, which is commonly ascribed to ZnO trap emission.[23,24,59] The case of the ZnO–ZA2–Au composite (Fig. 2–6A) demonstrates a rich set of emitting components, which appears to combine spectral signatures specific to both, pure and hybrid ZnO materials.

Spectral fitting suggests a unique resolving capacity. For example, our analysis of the spectrum in Fig. 2(2A) reveals that emission at about 530 ± 30 nm may be excited using different pathways: we may stimulate it using excitation at 340, 430, and 460 nm: see Fig. S9BB in SI file. Additionally, two-dimensional spectra of the selected samples demonstrate differences, which would not be noticeable while using conventional spectroscopy: for example, 1D spectral samplings would not allow identifying samples of nanoflowers, Fig. 2(5A) and platelets, Fig. 2(4A). Further, we note that fitting of two-dimensional spectra provides an opportunity to quantify energy flow. Specifically, comparing with emission of rhodamine 6G, we estimate quantum yields of CB → VB emission as 1.5×10^{-3}, 1.0×10^{-4}, 4.0×10^{-5}, 1.0×10^{-6}, 7.0×10^{-7}, 5.0×10^{-5} for the analytical standard, microspheres, nanorods, nanoplatelets, nanoflowers and ZnO–ZA2–Au composite, respectively. In the following, we review relaxation properties using relative quantum yield values, which are proportional to the evaluated absolutes values.

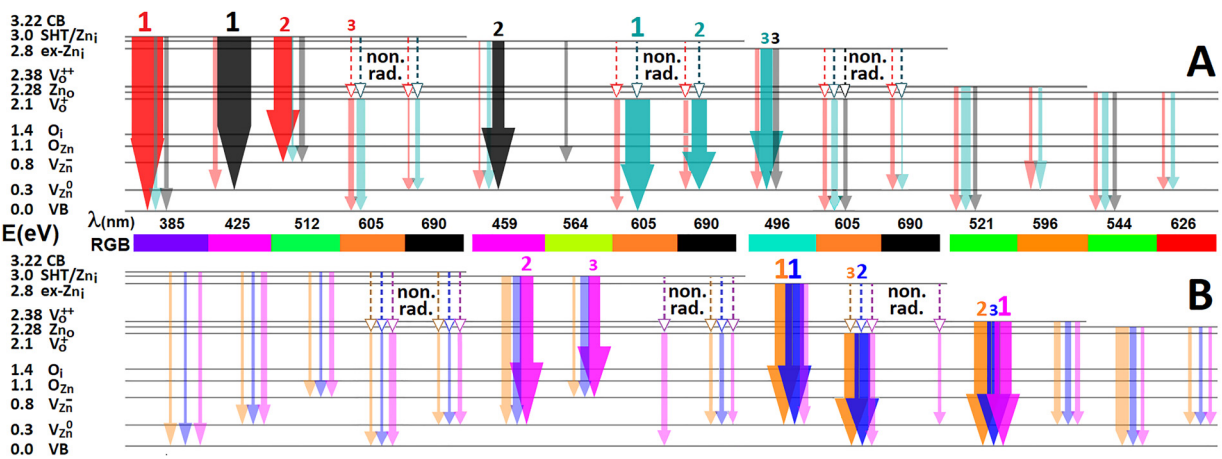

Fig. 3 Panel A: energy relaxation in pure ZnO materials: analytical standard (red), microsphere (black) and nanorod (cyan) *via* emission and non-radiative (non. rad.) pathways. Panel B: energy relaxation in hybrid ZnO systems: nanoplatelet (orange), nanoflower (blue) and Au including microstructure (magenta). Thickness of arrows is proportional to quantum yields, computed using 2D fitting protocol.[48] Numbers 1, 2 and 3 indicate leading, next and third relaxation pathway for the corresponding material according to color. We fade colors from weaker transitions.

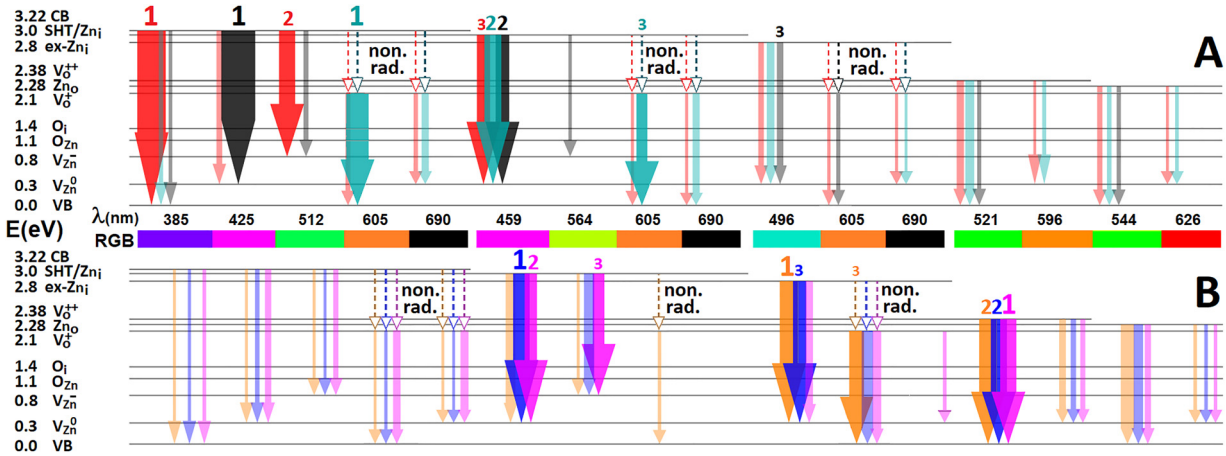

Fig. 4 PVA passivation effects. Panel A: energy relaxation in pure ZnO materials: analytical standard (red), microsphere (black) and nanorod (cyan) *via* emission and non-radiative (non. rad.) pathways. Panel B: energy relaxation in hybrid ZnO systems: nanoplatelet (orange), nanoflower (blue) and Au including microstructure (magenta).

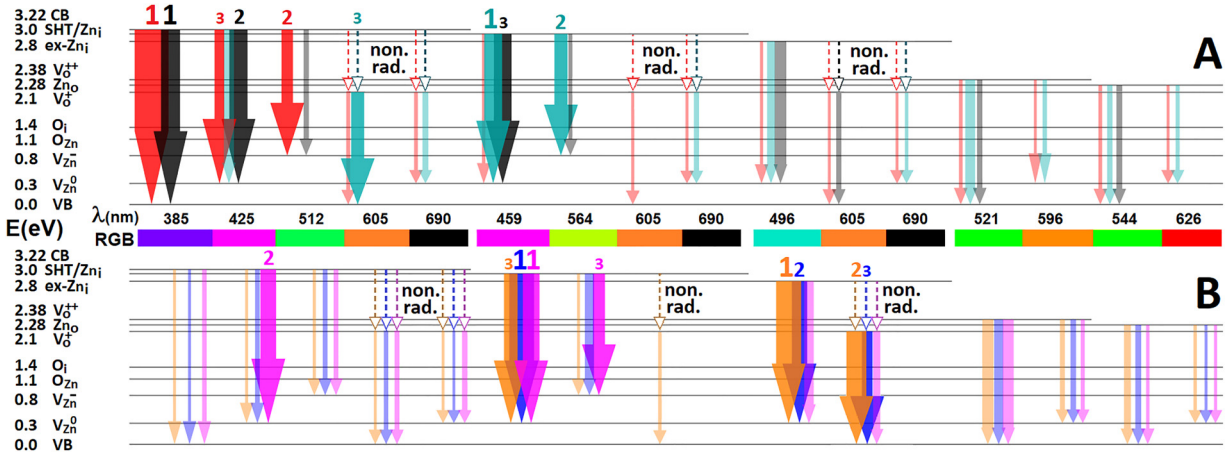

Fig. 5 $NaBH_4$ surface activation effects. Panel A: energy relaxation in pure ZnO materials: analytical standard (red), microsphere (black) and nanorod (cyan) *via* emission and non-radiative (non. rad.) pathways. Panel B: energy relaxation in hybrid ZnO systems: nanoplatelet (orange), nanoflower (blue) and Au including microstructure (magenta).

4. Discussion

4.1. Energy relaxation in pure and hybrid ZnO materials

For a convenience the energy levels in the energy relaxation diagrams (Fig. 3–5) are presented using straight lines at the levels corresponding to the minima and maxima of a corresponding band. To reflect different efficiencies, we use arrows with widths scaled according to relative quantum yields of the transitions, specific to each considered material.

According to the results of spectral fitting, in Fig. 3A and B we present energy relaxation diagrams for a ZnO standard, nanorod and microsphere and three hybrid ZnO materials, respectively. Numbers 1, 2 and 3 indicate leading, next and third relaxation pathway for the corresponding material according to color. We fade colors for the weaker transitions.

Comparing the relative contributions of the NBE emission generated by the CB → VB transition, it is observed that all ZnO structures have band-gap exciton emission, centered at *ca.* 372 nm (3.33 eV). The relative contributions for pure ZnO structures, such as the analytical standard, microspheres and nanorods, are 42, 1.2 and 2.7% respectively. In the case of hybrid nanoplatelets and nanoflowers, the role of exciton emission is nearly negligible, about 0.2% in both cases. Exciton contribution in hybrid ZnO microstructures with gold inclusions is about 1.5% of the emission. Dominance of the exciton emission in the analytical standard is due to both, the relatively large size of crystalline domains and small surface to volume ratio of this material.

Both the microspheres and analytical standard have low populations of V_O and Zn_O defects. Structurally most comparable, it may be expected that the NBE emission for these materials should be comparable; however, the microsphere sample is dominated by two transitions formally ascribed to

CB → V_{Zn}^{0} (30%), as well as to shallow trap (SHT) → V_{Zn}^{0} and Zn_i → V_{Zn}^{0} (13%) transitions. Dominance of these "blue" transitions (with wavelengths at about 425 and 459 nm) makes microspheres outstanding in the series of ZnO samples studied. As we reported previously, such emission may suggest the contribution of polariton phenomena due to the nearly ideal spherical cavity of the particles to trap light.[49] Polariton physics due to light entrapment in a particle as a cavity is outside the scope of linear spectroscopy, though the energy ladder to seed cavity modes does have its own contribution. The observed dominant contribution of SHT/Zn_i → V_{Zn}^{0} transitions suggests that the synthesis procedure used[78] stimulates nonuniform distributions of metal cations that leads to the co-presence of Zn interstitial and Zn vacancy defects. At the same time, apparently, both, the decrease of crystallinity and the relative increase of the outer surface contribute to the reduction of emissions.

Among the considered pure ZnO materials, the nanorod sample demonstrates the richest set of spectral components as shown in Fig. 2–2A. The role of the surface is likely important for this material form of ZnO. Emission of the system is dominated by V_O^{+} → VB, V_O^{+} → V_{Zn}^{0}, and ex-Zn_i → V_{Zn}^{-} transitions at about 605, 690 and 496 nm, respectively. In contrast to the other pure ZnO systems, nanorod photoluminescence is controlled by deep donors and Zn interstitial sites:[73–75] both regular and extended. The detected spectral superposition agrees with the emissive properties reported for well-faceted ZnO nanorods.[79]

Next, we consider the ZnO-hybrid systems, where ZnO is made in the presence of a peptide. Comparing emission spectra for similar pure ZnO nanorods (Fig. 2–2A) and unit elements of a ZnO flower (Fig. 2–5A) may suggest additional electronic controls in such sub-micron structures upon bioinorganic synthesis. Also, while the former is pure ZnO, the latter nanorod is a hybrid that involves the ZA2 polypeptide: the same ZA2 polypeptide participates in ZnO–ZA2–Au hybrids.

In contrast to the 'pure' ZnO materials, the hybrid systems demonstrate dominance of oxygen vacancies and extended zinc interstitials as the emitting sites, and zinc vacancies as accepting states. Thus, the hybrid systems show a strong tendency to emit green radiation of different origins: we refer to spectral components at 496, 564 and 521 nm, as shown in Fig. 3B.

This divide between the emissive patterns of pure and hybrid ZnO materials suggests that, during synthesis, the presence of polypeptides alters organization at the lattice level significantly. In particular, the polypeptides used in this study, GT16 (**GLHVMHKVA**PPRGGGC) and ZA2 (**GLHVMHKVA**YSSGAPPMPPF) are derived from the G-12 (**GLHVMHKVA**PPR) sequence reported to bind to ZnO.[80,81] Both, the G-12 and GT-16 sequences associate with (0001) and (10$\bar{1}$0) facets in the developing crystal, mediating growth along the *a* and *c* axes respectively.[80] However, the GT16 sequence preferentially binds to the (0001) plane restricting growth along the *c*-axis.[80] The facet preference for ZA2 polypeptide is not characterized; although, since the primary sequences share commonality over the 9 amino acids at the N-terminus, as a first approach, we may consider that binding of ZA2 polypeptide may follow tendencies similar to those described for the parental G-12 polypeptide. Indeed, Raman spectra (see Fig. S3 in SI file) indicate that, when next to a ZnO surface and in hybrid composites, G12, G16 and ZA2 polypeptides have similar Amide I signatures, which are typical for contributions of beta fold and random coil. Therefore, upon synthesis ZA2 may interact with both, (0001) and (10$\bar{1}$0) facets. The (0001) facet is a Zn^{2+} terminated surface, and the (10$\bar{1}$0) facet is a Zn^{2+} and O^{2-} mixed terminated surface, meaning that interactions with these surfaces may produce variant populations of Zn and O vacancies. If this is the case, such polypeptide induced defects would tend to be a volume specific property.

Quantitative consideration of the energy relaxation pathways for the hybrid systems shows the percentile contributions of the different transitions. Ex-Zn_i → V_{Zn}^{0} at about 496 nm is a dominant transition for the nanoplatelets and nanoflower materials contributing 23% of the total emission, in both cases. This transition is quite small (2 and 5%) in the analytical standard and in the microspheres but is a 13% contribution in the nanorod sample. The V_O^{+} → VB transition at 6 nm (see the thick orange, blue, magenta arrows next to the 496 nm set in Fig. 3B) plays the second and the third role for nanoflowers (19%) and platelets (17%), respectively. In contrast, for the ZnO–ZA2–Au system, the leading pathway for energy relaxation is V_O^{++} → VB emission with a relative yield of 21%. The same channel is secondary (22%) and tertiary (15%) for the platelets and nanoflowers, respectively. More curiously, shallow traps and Zn_i states are the second (16%) and the third (13%) leading pathways stimulating SHT/Zn_i → V_{Zn}^{0} and SHT/Zn_i → V_{Zn}^{-} transitions respectively: see magenta arrows at 459 and 564 nm, respectively, in Fig. 3B.

What makes the hybrid systems unique is that polypeptide participation enhances relaxation channels with participation of both, zinc interstitial (Zn_i and ex-Zn_i) and oxygen vacancy (V_O^{+} and V_O^{++}) as the most competitive emissive states. This lends some support to the idea that polypeptide mediation contributes to an increased contribution of these defects. However, while the 2DEM spectra of nanoplatelets and nanoflowers (see Fig. 2(4A) and (5A), respectively) demonstrate obvious similarities, ZnO–ZA2–Au composites demonstrate stronger contributions of the second "blue" excited emission set, indicating that, when available to interact with gold, the ZA2 polypeptide imposes less of a perturbation on the Zn^{2+} terminated (0001) facet.

In comparison, for both the analytical standard and microspheres, transitions with participation of zinc interstitial (ex-Zn_i) and oxygen vacancy (V_O^{+} and V_O^{++}) states contribute less than 5% into their total emission. However, for the nanorods the ex-Zn_i donors provide 13% of the total emission. This suggests that HMTA hydrothermal synthesis is more "unpredictable" in respect to a pure ZnO lattice, the larger the role of the surface. Also, this supports the fact that HMTA synthesis forming nanorods with a preferred direction of growth along the *c*-axis,[51] growth increases the contribution of the (10$\bar{1}$0) facet with its mixed terminations.[13,25]

Further, it is interesting to note that, while ZnO nanorods (Fig. 1(3A)) and the structural element of nanoflowers (Fig. 1(5A)) exhibit similar dimensions and the enhanced role of the surface, their emissive properties are different. Polypeptides involved in the synthesis play a distinct role that impacts how electronic properties compete with surface effects. Since there is a proposed impact on the population density of extended Zn interstitial states, ex-Zn_i, it is important to remember that these defects are usually associated with the volume of a ZnO structure.[82,83] If this is the case, we may suggest that polypeptides affect the volume lattice to the extent that its role in the electronics of the material becomes competitive in the systems, where surface effects are considered to dominate.

The complex interplay between defect states and resultant emissive transitions have been harnessed with a range of surface coatings reported in the literature targeting passivation or introduction of defect states.[52,53,82,83] From these reported surface treatments two are of particular interest: 0.5% PVA surface passivation,[52] and 1 M $NaBH_4$ surface activation, which is reported to increase oxygen vacancy defects at the surface.[53] In the following sections, we detail and discuss the effects of the two modifications.

4.2. PVA ''passivation''

Fitting two-dimensional spectra of PVA treated materials, as shown in Fig. 2(1B)–(6B) yields quantitative information expressed in the energy relaxation diagram presented in Fig. 4. The PVA treatment impacts emission of the nanorod and nanoflower samples and does not significantly affect energy relaxation in the other systems. Qualitatively this is obvious by a visual inspection comparing the spectral plots of the A and B sets of panels in Fig. 2.

This observation shows that PVA application has the most impact where the ratio of surface to volume is sufficiently high, Table 1. Considering this, next it is instructive to address the surface chemistry of the ZnO materials in the presence of PVA.

Following our assignments, under PVA nanorod photoluminescence is controlled by conducting band, V_{Zn}^-acceptors, and by both, regular and extended Zn_i sites. Considering the estimated energy flow redistribution, it seems that application of PVA depletes densities of ex-Zn_i (to be photoexcited), that relaxation changes along the non-radiative relaxation from CB to provide $V_O^+ \rightarrow$ VB (28%) main, and SHT/$Zn_i \rightarrow V_{Zn}^0$ secondary pathway, instead. This indicates possible correlation of donor and acceptor defects implying spatial inhomogeneities and distance (between donor and acceptor densities) effects, which is plausible upon structural confinement. We may suggest PVA hydroxyl moieties[84] participate in correlative restructuring of ex-Zn_i and V_O^+ oxygen vacancies and, possibly, stimulate a compensation of V_{Zn}^0. If such reorganizations occur, these would affect the analogous emission components in microspheres, but to a lesser extent due to the smaller surface to volume ratio in the microspheres. Concerning the role of the surface, here, it is instructive to review the effect of PVA application to nanoflowers, where structural elements are similar in dimension to the nanorods. According to our assignments, for this system, application of PVA depletes contribution of ex-Zn_i states analogously to the described passivation processes in nanorods. This suggests that similar shape and surface to volume ratio as anticipated for these two systems govern the involved defects densities.

Next, we use current examples to generalize the approach: according to our experimental observations and the fitting outcome, for all the considered cases under attention, PVA treatment is not observed to affect much the participation of V_O^{++} vacancies in the emission data. At the same time, if we compare a 1D spectrum (a vertical slice) excited at 3.3 eV for a ZnO nanorod sample as prepared and treated by PVA, we do observe the decay of the in-gap transition with a wavelength shift from near infra-red toward blue-green and red emission components (see cyan arrows change in Fig. 3 and 4 in respect to RGB code color bar), consistent with literature.[85] We believe, this is a good example to show that measuring and fitting 2DEM spectra is critically important for quantitative evaluation of different relaxation pathways, while accounting the full ladder of involved states.

4.3. $NaBH_4$ ''activation''

In Fig. 2(1C)–(6C) we present two-dimensional spectra of the materials after $NaBH_4$ treatment. From analysis of the data we show that both, the analytical standard and microspheres see an increase in exciton emission (at *ca.* 335 nm, 3.7 eV) from 42% to 69% and from 3% to 24%, respectively. The noticeable and significant redistributions of energy relaxations (in favor of the exciton emission) in the analytical standard and in microspheres are due to the slight attenuation of the CB $\rightarrow V_{Zn}^-$ transition and an abatement of the CB $\rightarrow V_{Zn}^0$ contribution, respectively.

Here, we would like to stress that the arrow thickness in Fig. 3–5 reflects relative quantum yield, not absolute yield. For example, the exciton emission in microspheres does not experience any enhancement upon $NaBH_4$ treatment, but its relative role in total energy relaxation increases (thickness of the black arrow #1 in Fig. 5A) because the originally dominant relaxation pathway CB $\rightarrow V_{Zn}^0$ gets quenched significantly: see panels 3A and 3C in Fig. 2.

In the case of ZnO nanorods, the sample demonstrates no exciton component when treated with $NaBH_4$: compare Fig. 3 and 5. Concurrently, the treatment leads to a complete attenuation of the main ''red'' and ''infrared'' emissions of the ''ultraviolet excited'' set. In result, there is a relative increase of the 564 nm ''yellow'' luminescence (from 10% to 15%), as well as the 459 nm ''ultraviolet'' (from 0% to 22%) emission components of the ''ultraviolet'' excitation set. According to our assignments, we ascribe this redistribution of energy flow in nanorods to a significant depletion of ex-Zn_i sites, and a decrease of regular Zn_i sites. Overall, in nanorods, the energy flow redistribution is similar regardless of PVA or $NaBH_4$ treatment. In both cases, we deal with the systems where surface plays a larger role. However, the nature of the agents is different.

To explain the observations in the pure ZnO systems under $NaBH_4$, we propose that as expected for this agent a reduction

process would provide partial compensation of positively charged defects and would induce possible restructuring to stimulate local Zn^0 clustering next to the surface that would involve merging of previously Zn^{2+} interstitial sites. Because of the small surface to volume ratio for the standard and microsphere samples, we may ascribe the effective reducing capacity of $NaBH_4$ to high diffusion mobility of hydrogen in this system with relatively small crystalline domains.[86]

Here, it is important to note that, in the case of pure ZnO systems, $V_O^{++} \rightarrow$ VB transition does not play any significant role (few percent in the standard and in the microspheres), but in nanorods, it accounts a 11% contribution. At the same time, in all pure ZnO structures, application of $NaBH_4$ does not affect the $V_O^{++} \rightarrow$ VB energy relaxation channel.

For the polypeptide mediated hybrid structures, when untreated, the leading terms of the ''blue'' excited set (496 nm ex-$Zn_i \rightarrow V_{Zn}^0$ and 605 nm ex-$Zn_i \sim V_O^+ \rightarrow$ VB), and the ''green'' excited set (521 nm $V_O^{++} \rightarrow$ VB) dominate in energy relaxation: see Fig. 3B. The role of these transitions, in particular, discriminate the behavior of platelets and nanoflower hybrids from the ZnO standard and microspheres, where the near band-gap terms dominate. When untreated, ZnO–ZA2–Au composites share with the other hybrids significance of the $V_O^{++} \rightarrow$ VB path with 495 nm $Zn_i \rightarrow V_{Zn}^0$ and 564 nm $Zn_i \rightarrow V_{Zn}^-$ pathways to play secondary and tertiary roles.

In the cases of platelets (orange arrows), upon $NaBH_4$ application, we do not observe any change for the leading ex-$Zn_i \rightarrow V_{Zn}^0$ emission, but ex-$Zn_i \sim V_O^+ \rightarrow$ VB and $V_O^{++} \rightarrow$ VB components become smaller, providing for the relative increase of the $Zn_i \rightarrow V_{Zn}^0$ ultraviolet emission at 459 nm. Overall, upon $NaBH_4$ treatment, 2DEM spectrum of the platelet sample shows it to be the most conservative: compare Fig. 2(4A) and (4C).

Under the same treatment of nanoflowers and ZnO–ZA2–Au composites, the main change is similar to that observed for the platelets: the 521 nm $V_O^{++} \rightarrow$ VB transition gets smaller and the 459 nm $Zn_i \rightarrow V_{Zn}^0$ ultraviolet emission becomes dominant. Accordingly, in the case of the nanoflowers sample, the relative contributions of the emissions stimulated photoexciting ex-Zn_i are attenuated. At the same time, for the ZnO–ZA2–Au composite, fitting suggests a relative enhancement (from 6% to 18%.) of the CB $\rightarrow V_{Zn}^0$ ultraviolet emission. For the other hybrid systems, the near band-gap emissions remain below a few percent, regardless of whether the samples are treated or not.

In contrast to the results of PVA treatment, when under $NaBH_4$, 2DEM spectra of nanorods and nanoflowers do not demonstrate changes to distinguish surface contributions. This we ascribe to $NaBH_4$ redox chemistry, which we consider affects structural properties of ZnO deep below the surface due to the high diffusion mobility of hydrogen.[86]

In general, as we evaluate, in all hybrid systems under $NaBH_4$, we may note a significant attenuation of the ''green'' excited set 521 nm radiative $V_O^{++} \rightarrow$ VB energy relaxation pathway, which plays a prominent role in energy relaxation of the untreated samples. Specifically, $V_O^{++} \rightarrow$ VB transition efficiency changes from 22% to 13% in platelets, from 15% to 10% in nanoflowers and from 21% to 13% in ZnO–ZA2–Au composites. This is contrary to the view that $NaBH_4$ may introduce oxygen vacancy defects.[53] Due to the reported redox chemistry of $NaBH_4$,[87,88] we would consider OH^- and H species and electron transfer mechanisms as having a role in passivating oxygen vacancies. Our perspective is based on analysis accounting the relative efficiency of relaxations stimulated to excite all available band-gap and in-gap transitions, as we detail in this contribution.

The examples of quantitative two-dimensional spectral analysis of pure and hybrid ZnO microstructures have provided an opportunity to generalise the energy ladder manifold specific to ZnO based materials. Energy relaxation pathways can be reviewed quantitatively in dependence on structure, crystallinity, role of surface and external modifications with a critical message that there is no unique source of a ''green'', or a ''blue'', a ''red'' emission in ZnO materials, but similar ''green'' or ''blue'' emissions due to different relaxation pathways under different excitations. Further, if a 2D sampling format is adopted, the generalised energy ladder manifold offers a convenient artificial intelligence format[48] to quantify and sort types and conditions of ZnO bulk and interfaces in nano and microelectronic devices.[13,16–20] Beside possible tailoring of electronic states, robust and selective ZnO emission was reported effective to contrast latent fingerprint on aluminum, stainless steel, clear and black glass surfaces.[89] Here, considering the sensitivity of ZnO to external factors, we may suggest that 2D excitation emission microscopy of ZnO treated fingerprints may provide detail on the chemistry and biochemistry of a person prior to the actual crime scene.

5. Conclusions

Adopting recently established quantitative 2DEM spectroscopy,[48] we address the electronic states and explore energy relaxation pathways within the band-gap of three pure ZnO systems and of three hybrid materials. Results of 2D spectral analysis does not support a perspective on any unique ''green'', or ''blue'', or ''red'' emission transition, but specifies a ZnO energy manifold, which provides at least five sets of pathways (we excite using different wavelengths) to emit colors, which are similar in some cases. We believe this approach is critically important to avoid ambiguity in analysis of electronic properties of zinc oxide and other semiconductors, which possess analogously intricate networks of energy relaxation pathways.

2D spectral fitting suggests that, in the analytical standard, the ultraviolet exciton band-gap component dominates in emission under all conditions. In the microspheres, CB $\rightarrow V_{Zn}^0$ and $Zn_i \rightarrow V_{Zn}^0$ transitions provide the observed diversity of high energy emissive components. In the case of pure ZnO nanorods, where the surface to volume ratio is higher, populated non-radiatively from zinc interstitials, ''red'' and ''infrared'' emissive transitions from oxygen vacancies $V_O^+ \rightarrow$ VB and $V_O^+ \rightarrow V_{Zn}^0$ govern the 2D spectrum. In a contrast to the pure ZnO systems, 2D spectra of polypeptide

mediated hybrid structures demonstrate ex-Zn_i → V_{Zn}^{0} and non-radiative populated V_O^{+} → VB transitions of the "blue" excited set, as well as the V_O^{++} → VB transition of the "green" excited set to govern energy relaxation. Since the surface to volume ratio for a pure ZnO nanorod and for a structural element of a nanoflowers are comparable, it is obvious that polypeptide mediated structures demonstrate unique deep in-gap opto-electric properties not attainable in pure ZnO systems.

Application of PVA to nanorod and hybrid systems tends to attenuate the lower energy donor defects to stimulate emission from higher energy donors. According to the observed spectral changes, we discuss PVA hydroxyl moieties[84] to participate in surface (and next to it) restructuring of zinc interstitials. Effects of $NaBH_4$ treatment demonstrate similar tendencies, however, these are less surface specific. In contrast to PVA, we consider $NaBH_4$ to initiate reduction processes to provide partial compensation of positively charged defects and consequently induce possible restructuring to stimulate local Zn^0 clustering next to surface to involve merging of previously Zn^{2+} interstitial sites, and to seed hydrogen to diffuse into volume.

Having elaborated examples to sort the nature of emissive states and quantify efficiency of relaxation along different pathways in dependence on structure, composition and external treatment, we suggest that two-dimensional excitation emission spectroscopy helpful for industrial applications to certify electronic states and conditions in the bulk and at interfaces in nano and microelectronic devices. Further, we report that that a combination of the approach with microscopy of ZnO treated latent fingerprints may be informative far beyond just a person's identification.

Author contributions

DJO: methodology, investigation, software, writing – review and editing; VVV: investigation, formal analysis, data curation, methodology, visualization, software, writing – original draft, review and editing; CCP: conceptualization, investigation, formal analysis, funding acquisition, supervision, writing – original draft, review and editing.

Conflicts of interest

There are no conflicts of interest to declare.

Data availability

The data supporting this article have been included as part of the supplementary information (SI). Supplementary information: details of synthesis procedures, X-Ray data, Raman spectra, side by side comparisons of 2D experimental and fitted spectra for the samples as synthesised and after PVA and $NaBH_4$ treatments, outline of our assignments of the observed electronic transitions based on literature precedence. See DOI: https://doi.org/10.1039/d6tc00969g.

Acknowledgements

The authors are grateful for support from the Air Force Office of Scientific Research under AFOSR Awards No. FA9550-1-16-0213, FA9550-1-20-0206 and FA9550-1-24-0274.

References

1 R. B. Heller, J. McGannon and A. H. Weber, Precision Determination of the Lattice Constants of Zinc Oxide, *J. App. Phys.*, 1950, **21**, 1283.
2 A. Cimino, M. Marezio and A. Santoro, Effect of additions on the lattice parameters of zinc oxide, *Die Naturwissenschaften*, 1957, **44**, 348.
3 R. A. Powell, W. E. Spicer and J. C. McMenamin, Photoemission Studies of Wurtzite Zinc Oxide, *Phys. Rev. B*, 1972, **6**, 3056.
4 V. Srikant and D. R. Clarke, On the optical band gap of zinc oxide, *J. App. Phys.*, 1998, **83**, 5447.
5 G. Heiland, E. Mollwo and F. Stöckmann, Electronic Processes in Zinc Oxide, *Solid State Phys.*, 1959, **8**, 191.
6 L. Yin, L. Zhang, F. Li and M. Yu, ZnO single crystals: Synthesis and characterization, *Mat. Res. Bull.*, 2005, **40**, 2219.
7 A. R. Nimbalkar and M. G. Patil, Synthesis of ZnO thin film by sol-gel spin coating technique for H_2S gas sensing application, *Phys. B*, 2017, **527**, 7.
8 Y. Zhang, M. K. Ram, E. K. Stefanakos and D. Yogi Goswami, Synthesis, Characterization, and Applications of ZnO Nanowires, *J. Nanomat.*, 2012, **2012**, 1.
9 J.-J. Dong, J. Wu, H.-Y. Hao, J. Xing, H. Liu and H. Gao, Synthesis of ZnO Nanocrystals and Application in Inverted Polymer Solar Cells, *Nanoscale Res. Lett.*, 2017, **12**, 529.
10 Y. Xi, C. G. Hu, X. Y. Han, Y. F. Xiong, P. X. Gao and G. B. Liu, Hydrothermal synthesis of ZnO nanobelts and gas sensitivity property, *Solid State Commun.*, 2007, **141**, 506.
11 B. Lin, Z. Fu and Y. Jia, Green luminescent center in undoped zinc oxide films deposited on silicon substrates, *App. Phys. Lett.*, 2001, **79**, 943.
12 S. A. M. Lima, F. A. Sigoli, M. Jafelicci Jr. and M. R. Davolos, Luminescent properties of lattice defect correlation in zinc oxide, *Int. J. Inorg. Mater.*, 2001, **3**, 749.
13 A. Abliz, *et al.*, Rational Design of ZnO:H/ZnO Bilayer Structure for High-Performance Thin-Film Transistors, *ACS Appl. Mater. Interfaces*, 2016, **8**, 7862.
14 Q. Li, S.-L. Chen and W.-C. Jiang, Durability of nano ZnO antibacterial cotton fabric to sweat, *J. Appl. Polym. Sci.*, 2007, **103**, 412.
15 H. Hong, F. Wang, Y. Zhang, S. A. Graves, S. B. Z. Eddine, Y. Yang, C. P. Theuer, R. J. Nickles, X. Wang and W. Cai, Red fluorescent zinc oxide nanoparticle: a novel platform for cancer targeting, *ACS Appl. Mater. Interfaces*, 2015, **7**, 3373.
16 K. Nomura, H. Ohta, K. Ueda, T. Kamiya, M. Hirano and H. Hosono, Thin-film transistor fabricated in single-crystalline transparent oxide semiconductor, *Science*, 2003, **300**, 1269.

17 B.-Y. Oh, M.-C. Jeong, T.-H. Moon, W. Lee, J.-M. Myoung, J.-Y. Hwang and D.-S. Seo, Transparent conductive Al-doped ZnO films for liquid crystal displays, *J. Appl. Phys.*, 2006, **99**, 124505.
18 Z. L. Wang and J. Song, Piezoelectric nanogenerators based on zinc oxide nanowire arrays, *Science*, 2006, **312**, 242.
19 S. Xu, Y. Qin, C. Xu, Y. Wei, R. Yang and Z. L. Wang, Self-powered nanowire devices, *Nat. Nanotechnol.*, 2010, **5**, 366.
20 X. Wang, C. J. Summers and Z. L. Wang, Large-Scale Hexagonal-Patterned Growth of Aligned ZnO Nanorods for Nano-optoelectronics and Nanosensor Arrays, *Nano Lett.*, 2004, **4**, 423.
21 J. Ewles and R. Whiddington, The cathodoluminescence of some common materials, *Proc. R. Soc. A*, 1938, **167**, 34.
22 J. T. Randall, General introduction. Some recent experiments in luminescence, *Trans. Faraday Soc.*, 1939, **35**, 2.
23 A. van Dijken, E. A. Meulenkamp, D. Vanmaekelbergh and A. Meijerink, Identification of the transition responsible for the visible emission in ZnO using quantum size effects, *J. Lumin.*, 2000, **90**, 123.
24 K. Vanheusden, C. H. Seager, W. L. Warren, D. R. Tallant, J. Caruso, M. J. Hampden-Smith and T. T. Kodas, Green photoluminescence efficiency and free-carrier density in ZnO phosphor powders prepared by spray pyrolysis, *J. Lumin.*, 1997, **75**, 11.
25 H. Zeng, G. Duan, Y. Li, S. Yang, X. Xu and W. Cai, Blue Luminescence of ZnO Nanoparticles Based on Non-Equilibrium Processes: Defect Origins and Emission Controls, *Adv. Funct. Mater.*, 2010, **20**, 561.
26 R. Raji and K. G. Gopchandran, ZnO nanostructures with tunable visible luminescence: Effects of kinetics of chemical reduction and annealing, *J. Sci.: Adv. Mater. Dev.*, 2017, **2**, 51.
27 Ü. Özgür, Y. I. Alivov, C. Liu, A. Teke, M. A. Reshchikov, S. Doğan, V. Avrutin, S.-J. Cho and H. Morkoç, A comprehensive review of ZnO materials and devices, *J. Appl. Phys.*, 2005, **98**, 041301.
28 A. B. Djurišić, X. Liu and Y. H. Leung, Zinc oxide films and nanomaterials for photovoltaic applications, *Phys. Status Solidi RRL*, 2014, **8**, 123.
29 S. J. Pearton and F. Ren, Advances in ZnO-based materials for light emitting diodes, *Curr. Opin. Chem. Eng.*, 2014, **3**, 51.
30 R. K. Biroju and P. K. Giri, Strong visible and near infrared photoluminescence from ZnO nanorods/nanowires grown on single layer graphene studied using sub-band gap excitation, *J. Appl. Phys.*, 2017, **122**, 044302.
31 G. Mie, Beiträge zur Optik trüber Medien, speziell kolloidaler Metallösungen, *Ann. Phys.*, 1908, **330**, 377.
32 S. A. Maier, *Plasmonics: Fundamentals and Applications*, Springer: New York, 2007.
33 T. Chen, G. Z. Xing, Z. Zhang, H. Y. Chen and T. Wu, Tailoring the photoluminescence of ZnO nanowires using Au nanoparticles, *Nanotechnology*, 2008, **19**, 435711.
34 J. Im, J. Singh, J. W. Soares, D. M. Steeves and J. E. Whitten, Synthesis and Optical Properties of Dithiol-Linked ZnO/Gold Nanoparticle Composites, *J. Phys. Chem. C*, 2011, **115**, 10518.
35 S. Park, Y. Mun, S. An, W. Lee and C. Lee, Enhanced photoluminescence of Au-functionalized ZnO nanorods annealed in a hydrogen atmosphere, *J. Lumin.*, 2014, **147**, 5.
36 L. Su and N. Qin, A facile method for fabricating Au-nanoparticles-decorated ZnO nanorods with greatly enhanced near-band-edge emission, *Ceram. Int.*, 2015, **41**, 2673.
37 T. Bora, H. H. Kyaw, S. Sarkar, S. K. Pal and J. Dutta, Highly efficient ZnO/Au Schottky barrier dye-sensitized solar cells: Role of gold nanoparticles on the charge-transfer process, *Beil. J. Nanotechnol.*, 2011, **2**, 681.
38 M. Ahmad, S. Yingying, A. Nisar, H. Sun, W. Shen, M. Wei and J. Zhu, Synthesis of hierarchical flower-like ZnO nanostructures and their functionalization by Au nanoparticles for improved photocatalytic and high performance Li-ion battery anodes, *J. Mater. Chem.*, 2011, **21**, 7723.
39 W. L. Ong, S. Natarajan, B. Kloostra and G. W. Ho, Metal nanoparticle-loaded hierarchically assembled ZnO nanoflakes for enhanced photocatalytic performance, *Nanoscale*, 2013, **5**, 5568.
40 M. Wu, W.-J. Chen, Y.-H. Shen, F.-Z. Huang, C.-H. Li and S.-K. Li, In situ growth of matchlike ZnO/Au plasmonic heterostructure for enhanced photoelectrochemical water splitting, *ACS Appl. Mater. Interfaces*, 2014, **6**, 15052.
41 F.-X. Xiao and B. Liu, In situ etching-induced self-assembly of metal cluster decorated one-dimensional semiconductors for solar-powered water splitting: unraveling cooperative synergy by photoelectrochemical investigations, *Nanoscale*, 2017, **9**, 17118.
42 Y. K. Mishra, S. Mohapatra, R. Singhal, D. K. Avasthi, D. C. Agarwal and S. B. Ogale, Au–ZnO: A tunable localized surface plasmonic nanocomposite, *Appl. Phys. Lett.*, 2008, **92**, 043107.
43 L. Chen, L. Luo, Z. Chen, M. Zhang, J. A. Zapien, C. Sing, L. Shuit and T. Lee, ZnO/Au Composite Nanoarrays As Substrates for Surface-Enhanced Raman Scattering Detection, *J. Phys. Chem. C*, 2010, **114**, 93.
44 S. Adesoye, S. Al Abdullah, A. Kumari, G. Pathiraja, K. Nowlin and K. Dellinger, Au-Coated ZnO Surface-Enhanced Raman Scattering (SERS) Substrates: Synthesis, Characterization, and Applications in Exosome Detection, *Chemosensors*, 2023, **11**, 554.
45 A. Chantaraklud, C. Rattanabut, S. Bamrungsap and T. Bora, Light-driven in situ deposited Au nanoparticles on ZnO substrate with ultrasensitive SERS enhancement for molecular detection, *Mikrochim. Acta*, 2025, **192**, 277.
46 D. J. Oliver, V. V. Volkov and C. C. Perry, ZnO Nanogold Doping: A Bioinorganic Paradigm for Sensing and Optical Security Applications, *ACS Appl. Nano Mater.*, 2021, **4**, 14241.
47 L. J. Brillson and Y. Lu, ZnO Schottky barriers and Ohmic contacts Available to Purchase, *J. Appl. Phys.*, 2011, **109**, 121301.
48 D. J. Oliver, V. V. Volkov and C. C. Perry, Solid State Excitation-Emission Spectroscopy for the Non-Destructive

Analysis of Band-Gap & Defect States in Inorganic and Organic Semiconductors, *Adv. Mater. Interfaces*, 2022, **10**, 2202048.

49 V. V. Volkov, D. J. Oliver and C. C. Perry, Polariton condensation and surface enhanced Raman in spherical ZnO microcrystals, *Nat. Commun.*, 2020, **11**, 4908.

50 M.-K. Liang, M. J. Limo, A. Sola-Rabada, M. J. Roe and C. C. Perry, New Insights into the Mechanism of ZnO Formation from Aqueous Solutions of Zinc Acetate and Zinc Nitrate, *Chem. Mater.*, 2014, **26**, 4119.

51 M. J. Limo and C. C. Perry, Thermodynamic Study of Interactions Between ZnO and ZnO Binding Peptides Using Isothermal Titration Calorimetry, *Langmuir*, 2015, **31**, 6814.

52 L. Qin, C. Shing, S. Sawyer and P. S. Dutta, Enhanced ultraviolet sensitivity of zinc oxide nanoparticle photoconductors by surface passivation, *Opt. Mater.*, 2011, **33**, 359.

53 X.-F. Su, J.-B. Chen, R.-M. He, Y. Li, J. Wang and C.-W. Wang, The preparation of oxygen-deficient ZnO nanorod arrays and their enhanced field emission, *Mat. Sci. Semicond. Processing*, 2017, **67**, 55.

54 A. L. Patterson, *Phys. Rev.*, 1939, **56**, 978.

55 P. S. Xu, Y. M. Sun, C. S. Shi, F. Q. Xu and H. B. Pan, The electronic structure and spectral properties of ZnO and its defects, *Nucl. Instrum. Methods Phys. Res., Sect. B*, 2003, **199**, 286.

56 K. Lawson-Wood, S. Upstone and K. Evans, *Determination of Relative Fluorescence Quantum Yields using the FL6500 Fluorescence Spectrometer*, PerkinElmer Inc., 2018.

57 N. J. Everall, *Handbook of Vibrational Spectroscopy*, John Wiley & Sons, Ltd., 2006, vol. 141.

58 M. Šćepanović, M. Grujić-Brojčin, K. Vojisavljević, S. Bernik and T. Srećković, Raman study of structural disorder in ZnO nanopowders, *J. Raman Spec.*, 2010, **41**, 914.

59 F. A. Kröger and H. J. Vink, The Origin of the Fluorescence in Self-Activated ZnS, CdS, and ZnO, *J. Chem. Phys.*, 1954, **22**, 250.

60 D. C. Reynolds, C. W. Litton and T. C. Collins, Zeeman Effects in the Edge Emission and Absorption of ZnO, *Phys. Rev.*, 1965, **140**, A1726.

61 D. McCluskey, S. J. Jokela, K. K. Zhuravlev, P. J. Simpson and K. G. Lynn, Infrared spectroscopy of hydrogen in ZnO, *Appl. Phys. Lett.*, 2002, **81**, 3807.

62 C. G. Van de Walle, Hydrogen as a cause of doping in zinc oxide, *Phys. Rev. Lett.*, 2000, **85**, 1012.

63 D. M. Hofmann, A. Hofstaetter, F. Leiter, H. Zhou, F. Henecker, B. K. Meyer, S. B. Orlinskii, J. Schmidt and P. G. Baranov, Hydrogen: a relevant shallow donor in zinc oxide, *Phys. Rev. Lett.*, 2002, **88**, 045504.

64 E. V. Lavrov, J. Weber, F. Börrnert, C. G. van de Walle and R. Helbig, Hydrogen-related defects in ZnO studied by infrared absorption spectroscopy, *Phys. Rev. B: Condens. Matter Mater. Phys.*, 2002, **66**, 165205.

65 B. K. Meyer, H. Alves, D. M. Hofmann, W. Kriegseis, D. Förster, F. Bertram, J. Christen, A. Hoffmann, M. Straßburg, M. Dworzak, U. Haboeck and A. V. Rodina, Bound exciton and donor–acceptor pair recombinations in ZnO, *Phys. Status Solidi B*, 2004, **241**, 231.

66 D. M. Hofmann, D. Pfisterer, J. Sann, B. K. Meyer, R. Tena-Zaera, V. Munoz-Sanjose, T. Frank and G. Pensl, Properties of the oxygen vacancy in ZnO, *Appl. Phys. A: Mater. Sci. Proc.*, 2007, **88**, 147.

67 C. H. Ahn, Y. Y. Kim, D. C. Kim, S. K. Mohanta and H. K. Cho, A comparative analysis of deep level emission in ZnO layers deposited by various methods, *J. Appl. Phys.*, 2009, **105**, 013502.

68 H. Zeng, G. Duan, Y. Li, S. Yang, X. Xu and W. Cai, Blue Luminescence of ZnO Nanoparticles Based on Non-Equilibrium Processes: Defect Origins and Emission Controls, *Adv. Funct. Mater.*, 2010, **20**, 561.

69 H. He, Y. Wang, J. Wanga and Z. Ye, Extraction of the surface trap level from photoluminescence: a case study of ZnO nanostructures, *Phys. Chem. Chem. Phys.*, 2011, **13**, 14902.

70 F. Kayaci, S. Vempati, I. Donmez, N. Biyikli and T. Uyar, Role of zinc interstitials and oxygen vacancies of ZnO in photocatalysis: a bottom-up approach to control defect density, *Nanoscale*, 2014, **6**, 10224.

71 W. R. L. Lambrecht, A. Rodina, S. Limpijumnong, B. Segall and B. Meyer, Valence-band ordering and magneto-optic exciton fine structure in ZnO, *Phys. Rev. B: Condens. Matter Mater. Phys.*, 2002, **65**, 075207.

72 B. Gil, Oscillator strengths of A, B, and C excitons in ZnO films, *Phys. Rev. B: Condens. Matter Mater. Phys.*, 2001, **64**, 201310(R).

73 A. Janotti and C. G. Van de Walle, Native point defects in ZnO, *Phys. Rev. B: Condens. Matter Mater. Phys.*, 2007, **76**, 165202.

74 F. Oba, M. Choi, A. Togo and I. Tanaka, Point defects in ZnO: an approach from first principles, *Sci. Technol. Adv. Mater.*, 2011, **12**, 034302.

75 Y. Yang, Y. Zhang, S. Fernandez-Alberti and R. Long, *J. Phys. Chem. Lett.*, 2024, **15**, 1.

76 S. B. Zhang, S. H. Wei and A. Zunger, Intrinsic n-type versus p-type doping asymmetry and the defect physics of ZnO, *Phys. Rev. B: Condens. Matter Mater. Phys.*, 2001, **63**, 075205.

77 H. Morkoç and Ü. Özgür, *Zinc Oxide: Fundamentals, Materials and Device Technology*, John Wiley & Sons, 2008.

78 R. S. Moirangthem, P.-J. Cheng, P. C.-H. Chien, B. T. H. Ngo, S.-W. Chang, C.-H. Tien and Y.-C. Chang, Optical cavity modes of a single crystalline zinc oxide microsphere, *Opt. Exp.*, 2013, **21**, 3010.

79 E. De la Rosa, S. Sepúlveda-Guzman, B. Reeja-Jayan, A. Torres, P. Salas, N. Elizondo and M. Jose Yacaman, Controlling the Growth and Luminescence Properties of Well-Faceted ZnO Nanorods, *J. Phys. Chem. C*, 2007, **111**, 8489.

80 M.-K. Liang, O. Deschaume, S. V. Patwardhan and C. C. Perry, Direct evidence of ZnO morphology modification via the selective adsorption of ZnO-binding peptides, *J. Mater. Chem.*, 2011, **21**, 80.

81 M. M. Tomczak, M. K. Gupta, L. F. Drummy, S. M. Rozenzhak and R. R. Naik, Morphological control and assembly of zinc oxide using a biotemplate, *Acta Biomater.*, 2009, **5**, 876.

82 P. Erhart and K. Albe, Diffusion of zinc vacancies and interstitials in zinc oxide, *Appl. Phys. Lett.*, 2006, **88**, 201918.
83 A. Ali, G. Rahman, T. Ali, M. Nadeem, S. K. Hasanain and M. Sultan, . Enhanced band edge luminescence of ZnO nanorods after surface passivation with ZnS, *Phys. E*, 2018, **103**, 329.
84 S. Okeil, S. Rabet, G. V. Huerta, G. Raabe and G. Garnweitner, Understanding the Role of Solvent on the Growth of Zinc Oxide: Insight from Experiment and Molecular Dynamics Simulations, *Langmuir*, 2024, **40**, 19343.
85 J. A. Röhr, J. Sá and S. J. Konezny, The role of adsorbates in the green emission and conductivity of zinc oxide, *Commun. Chem.*, 2019, **2**, 52.
86 M. G. Wardle, J. P. Goss and P. R. Briddon, First-Principles Study of the Diffusion of Hydrogen in ZnO, *Phys. Rev. Lett.*, 2006, **96**, 205504.
87 G. Guella, C. Zanchetta, B. Patton and A. Miotello, New Insights on the Mechanism of Palladium-Catalyzed Hydrolysis of Sodium Borohydride from 11B NMR Measurements, *J. Phys. Chem. B*, 2006, **110**, 17024.
88 Y. Zhou, C. Fang, Y. Fang, F. Zhu, H. Liu and H. Ge, Hydrogen generation mechanism of BH_4^- spontaneous hydrolysis: A sight from ab initio calculation, *Int. J. Hydrogen Energy*, 2016, **41**, 22668.
89 B. Flores, M. Guzman, R. Grieseler, A. Quiroz, L. Malet and S. Godet, Synthesis of Zinc Oxide Nanoparticles and Their Potential Application in the Detection of Latent Fingerprints, *J. Clust. Sci.*, 2025, **36**, 70.